Magnetic and magnetotransport properties of $GdBaCo_2O_{5+\delta}$: A high magnetic-field study

Marc Respaud,[1] Carlos Frontera,[2] José Luis García-Muñoz,[2] Miguel Ángel G. Aranda,[3] Bertrand Raquet,[1] Jean Marc Broto,[1] Harison Rakoto,[4] Michel Goiran,[4] Anna Llobet,[5] and Juan Rodríguez-Carvajal[6]

[1]*LPMC, INSA, 135 avenue de Rangueil, Toulouse, 31077 France*

[2]*Institut de Ciència de Materials de Barcelona, CSIC, Campus de la UAB, E-08193 Bellaterra, Spain*

[3]*Departamento de Química Inorgánica, Cristalografía y Mineralogía, Universidad de Málaga, 29071 - Málaga, Spain*

[4]*LNCMP, 147 avenue de Rangueil, Toulouse, 31077 France*

[5]*Laboratoire de Magnetisme Louis Néel, CNRS 25 Avenue des Martyrs - BP 166, 38042 Grenoble Cedex 9, France*

[6]*Laboratoire Léon Brillouin, CEA-CNRS, Centre d'Etude de Saclay, Gif sur Yvette Cedex, 91191 France*

(Received 20 December 2000; revised manuscript received 18 June 2001; published 31 October 2001)

Magnetic, transport, and optical measurements performed on $GdBaCo_2O_{5.5}$ under pulsed magnetic fields up to 35 T have allowed us to determine its complete $\mu_0 H$-T phase diagram. A first-order field-induced transition takes place below the Néel point ($T_N \approx 255$ K), which implies the appearance of a ferromagnetic component and steep changes in the conductivity. The ferromagnetic component $(0.45 \pm 0.1)\mu_B$/(Co ion) does not appreciably change below T_N. The nature of the high-field ferromagnetic state is discussed in connection with the zero-field ferromagnetic (or ferrimagnetic) phase above T_N.

DOI: 10.1103/PhysRevB.64.214401 PACS number(s): 75.50.Dd, 75.30.Vn, 71.27.+a

I. INTRODUCTION

Cobalt oxides with perovskite structure form a very rich family of compounds that have been extensively studied during the second half of the 20th century.[1–9] Its interest comes not only from a fundamental point of view, but also from technological aspects. They present rich phase diagrams and even giant magnetoresistance, with magnetoresistance values in some cases larger than 30%. An extensive work has been done on La-based cobaltites, both undoped ($LaCoO_3$, La_2CoO_4) or (Sr,Ca)-doped ($La_{1-x}Sr_xCoO_3$, $La_{2-x}Sr_xCoO_4$, $La_{1-x}Ca_xCoO_3$, $La_{2-x}Ca_xCoO_4$). Mainly devoted to the determination of the magnetic ground state, these studies show that the magnetism of the cobalt ions is far from simple and that determining the spin state of Co^{3+} ions has revealed to be a complex task. Since the crystal field (Δ_{CEF}) and the intra-atomic exchange energies (J_H) are comparable, a high-spin (HS) state ($t_{2g}^4 e_g^2, S=2$) and low-spin (LS) state ($t_{2g}^6 e_g^0, S=0$), as well as an intermediate-spin (IS) state ($t_{2g}^5 e_g^1, S=1$) can be observed depending on the ratio of Δ_{CEF} and J_H. A representative example can be found in the parent compound $LaCoO_3$ (only Co^{3+} ions in octahedra), in which two spin-state transitions have been reported. Both transitions are very extended in temperature. The first one happens between 20 and 100 K and the second one, which coincides with a metal-insulator transition, takes place between 450 and 600 K. There is a general consensus on the fact that at low temperature, below the first transition, Co^{3+} ions are in the LS state.[3,6–9] However, the other two spin states have been the subject of a great controversy. Señaris-Rodríguez and Goodenough stated in Ref. 3 that for 100 K$\leqslant T \leqslant$450 K half of the Co^{3+} ions are in LS and the other half in HS state forming a (short-range) ordered semiconductive phase. They also concluded that above 600 K there is long-range order of Co^{3+} ions in HS (50%) and IS states. Contrarily, neutron diffraction results ruled out this ordered scheme above 600 K.[4] The presence of Co^{3+} ions in the IS state has been confirmed by infrared spectroscopy.[8]

More recently, a great interest has appeared on rare-earth-based cobaltites doped with Ba: $LBaCo_2O_{5+\delta}$ with $L \equiv$ rare earth and $0 \leqslant \delta \leqslant 1$. They present several fascinating features with structural, spin-state, metal-insulator, and magnetic-field-induced transitions, as well as charge and orbital ordering phenomena.[10–19] In these compounds the oxygen content δ controls the mixed valence state of Co ions. The mean valence of Co varies from 2.5+ for $\delta=0$ to 3.5+ for $\delta=1$. Thus, for $\delta=1$ ($\delta=0$) Co^{3+} and Co^{4+} (Co^{2+}) are present in the same amount, while for $\delta=0.5$ only Co^{3+} is expected. In a very complete paper, Maignan *et al.*[14] showed that in polycrystalline compounds sintered in air under similar conditions, δ depends on the size of the lanthanide: the larger this size is, the larger δ is. Samples with $\delta=0$ present a comparatively large resistivity[14] and, at low temperature, a charge ordering of the Co^{3+}/Co^{2+} ions (at least for $L=$Y and Ho).[16,17] As happens for $LaCoO_3$, there is also some controversy about the spin state of Co in $LBaCo_2O_{5+\delta}$ compounds with $\delta=0$. Neutron diffraction data suggests that Co^{3+} ions in the pyramidal environment of $LBaCo_2O_5$ ($L=$Y, Ho) (Ref. 16 and 17) adopt a HS state even at low temperature. From electronic structure calculations for $YBaCo_2O_5$, a weak CF and the HS state for Co^{3+} and Co^{2+} has been theoretically predicted by Wu.[20] For the same compound, similar calculations reported in Ref. 21 predict the HS (IS) state for Co^{2+} (Co^{3+}). Moreover, Kwon and Min suggest that, for Co^{3+} sites, the orbital moment is only partially quenched in $YBaCo_2O_5$, rendering $\mu_s = 1.84\mu_B$ and $\mu_L = 0.40\mu_B$ for the spin and orbital moments.

The resistivity is considerably smaller in compounds with $\delta \lesssim 1$ for a wide range of lanthanides (at least from Gd to La).[11,14] In the middle, compounds with $\delta \approx 0.5$ present a metal-insulator transition at a temperature T_{MI} between 280 and 400 K (depending on the rare earth).[14] $LBaCo_2O_{5+\delta}$ perovskites consist in consecutive ordered layers of $[CoO_2]$-$[BaO]$-$[CoO_2]$-$[LO_\delta]$. For $\delta=0.5$ Moritomo *et*

al.[18] have described the structure of $TbBaCo_2O_{5.5}$ with the apical oxygen atoms and vacancies located in rows parallel to *a* which alternate along *b* and *c*. In this structure (*P mmm* crystal symmetry) CoO_6 octahedra (50%) and CoO_5 pyramids (50%) are ordered and occupy alternating planes along *b*. It has been reported in Ref. 18 that Co^{3+} ions undergo a spin-state transition at T_{MI}. Upon cooling, a long-range ferromagnetic (FM) moment appears below 300 K and suddenly disappears at $T_N = 260$ K, below which new magnetic Bragg peaks appear in the neutron diffraction patterns evidencing an antiferromagnetic (AFM) order.[18]

Measurements under high magnetic fields have revealed to be very useful in order to investigate the stability of charge- and orbital-ordered phases in oxides.[22–24] Magnetic-field-induced transitions on the resistivity and magnetization curves have been reported on $\delta \simeq 0.5$ Ba cobaltites below T_N.[11,12,22] A partial $\mu_0 H$-T macroscopic phase diagram was determined in Refs. 11,12, and 19 up to 14 T, although a microscopic interpretation of the first-order field transition is still lacking. The purpose of the present work has been to get insight into the electric and magnetic transitions of $GdBaCo_2O_{5+\delta}$ with $\delta \approx 0.5$. With this objective in mind, magnetization, magnetotransport, and far-infrared transmission measurements have been performed under high magnetic fields up to $\mu_0 H = 35$ T. They, together with some structural data, have permitted us to establish the $\mu_0 H$-T phase diagram and give a microscopic description of the temperature evolution of this oxide.

II. EXPERIMENTAL DETAILS

Polycrystalline $GdBaCo_2O_{5+\delta}$ was prepared by solid-state reaction in air. High-purity powders of Gd_2O_3, $BaCO_3$, and Co_3O_4 were mixed at stoichiometric weights. After a de-carbonation process, the mixture was pressed into a pellet and annealed during 24 h at 1125 °C in air. After a regrinding of the resulting pellet, the compression and annealing (at 1125 °C in air) processes were repeated several times. Synchrotron x-ray powder diffration data were collected at room temperature (RT) at the BM16 beamline of the European Synchrotron Radiation Facility (ESRF, Grenoble) using $\lambda = 0.442\,377$ Å. It is known that the oxygen content of air-synthesized $LBaCo_2O_{5+\delta}$ decreases increasing the size of the lanthanide and it is $\delta \approx 0.5$ for $L = Gd$.[14] As detailed latter, the refinement of the very-high-resolution synchrotron data determined the oxygen content $\delta = 0.54(3)$. Magnetic data at low field were taken in the temperature range 10 K $\leqslant T \leqslant 850$ K using an extraction magnetometer. High-magnetic-field magnetization measurements have been performed at the facilities of the SNCMP in Toulouse (France), between 4.2 and 300 K. Using the discharge of a bank capacitor in a coil, pulsed fields up to 35 T are obtained with a duration time of more that 1 s. The magnetization was measured by inductive methods using a system of two concentric pickup coils in opposition. The measured signal dM/dt is then integrated numerically. The conventional four-probe method in dc configuration was used to measure the resistivity and its magnetic field dependence for reasonable sample resistances ($R \lesssim 10^7\ \Omega$). In the insulating regime, magnetotransport data were obtained by measuring the magnetoconductivity. Far-infrared transmission measurements were carried out in the Faraday configuration using the same pulsed magnetic field. These measurements were done at a single frequency ($f = 344$ GHz) produced by a far-infrared Fabry-Perot cavity optically pumped by CO_2. Each spectrum corresponded to the sample transmission variation versus the applied magnetic field.

III. RESULTS

The high absorption of neutrons by natural Gd precludes a neutron diffraction investigation of the present compound. Ultrahigh-resolution synchrotron x-ray diffraction data show a single phase, free of impurities. The sample is very well crystallized, the diffraction peaks being remarkably sharp. The structural refinement of the RT data was consistent with a *P mmm* space group in which the perovskite cell doubled along *c* is also doubled along *b* due to the alternation of oxygen-rich and -deficient *a*-*c* layers. As expected, Gd and Ba ions are arranged in consecutive (0 0 1) layers; the oxygen vacancies are located in the Gd layers and ordered in alternating [1 0 0] rows. Thus, (0 1 0) planes of CoO_6 octahedra alternate with (0 1 0) planes of CoO_5 pyramids as has been described for $TbBaCo_2O_{5.5}$ and other $\delta \simeq 0.5$ compounds.[14,18] The refined atomic positions were the following: Ba $2o$ $(\frac{1}{2},0.2500(2),0)$, Gd $2p$ $(\frac{1}{2},0.2278(2),\frac{1}{2})$, Co1 $2r$ $(0,\frac{1}{2},0.2561(4))$; Co2 $2q$ $(0,0,0.2522(5))$; O1 $1a$ $(0,0,0)$; O2 $1e$ $(0,\frac{1}{2},0)$; O3 $1g$ $(0,\frac{1}{2},\frac{1}{2})$ [occupation factor $=0.08(3)$]; O4 $1c$ $(0,0,\frac{1}{2})$; O5 $2s$ $(\frac{1}{2},0,0.274(2))$; O6 $2t$ $(\frac{1}{2},\frac{1}{2},0.313(2))$; O7 $4u$ $(0,0.255(1),0.293(1))$. The model is very similar to that given in Ref. 18 (octahedra chains along *c*, alternating with corner-sharing square pyramids along *b*), but with the oxygen vacancies at $(0,\frac{1}{2},\frac{1}{2})$ instead of $(0,0,\frac{1}{2})$. The refinement of the oxygen occupancy indicates $\delta = 0.54(3)$, confirming the expected oxygen content. Moreover, regarding the data of Ref. 14 which correlates the unit cell parameters of $GdBaCo_2O_{5+\delta}$ samples with different oxygen contents, our RT unit cell parameters agree with the refined oxygen composition. Together with the lattice parameters, the main Co-O and Co-O-Co bond angles obtained at RT are also listed in Table I. By examining the Co-O bond lengths, it is apparent that the pyramidal environment of Co^{3+} sites in $GdBaCo_2O_{5.5}$ is rather different to the reported one for Co^{3+} sites in $YBaCo_2O_5$.[16] We observe an appreciable deformation in the basal plane of the pyramids compatible with the presence of Co^{3+} in the IS state ($t_{2g}^5 e_g^1$) at RT. However, such deformation is sensibly smaller than in the pyramids of $YBaCo_2O_5$. The relevance of the changes in the coordination environment of the pyramids with δ for the ground state of Co is not easy to elucidate.

Figure 1 shows the variation of the magnetization $[M(T)]$ in a field of 1 T as a function of the temperature (2–850 K) measured after a zero-field-cooling (ZFC) process. Upon cooling the system undergoes several successive magnetic transitions. The first one, which occurs at 360 K, leads to a sudden change in the slope of the $M^{-1}(T)$ curve. It has been reported that this change coincides with a metal-insulator

TABLE I. Lattice constants and main Co-O bond distances and angles for $GdBaCo_2O_{5.5}$ at RT obtained from synchrotron powder diffraction Rietveld refinements. Co-Oi stands for the bond lengths along $i=a,b$, and c axes. Co1 and Co2 correspond to, respectively, pyramids and octahedra.

Cell	a (Å)	b (Å)	c (Å)	V (Å^3)	R_F (%)
	3.87738(3)	7.82690(7)	7.53487(6)	228.667(5)	3.91
Pyramids	Co1-Oa ($\times 2$)	Co1-Ob ($\times 2$)	Co1-Oc	Co1-Oc′	$\langle$Co1-O$\rangle$
	1.986(3)	1.939(9)	1.929(3)	–	1.956
Octahedra	Co2-Oa ($\times 2$)	Co2-Ob ($\times 2$)	Co2-Oc	Co2-Oc′	$\langle$Co1-O$\rangle$
	1.945(1)	2.017(9)	1.901(3)	1.867(3)	1.949
$\theta_{\text{Co-O-Co}}$	Co1-Oa-Co1	Co2-Oa-Co2	Co1-Ob-Co2		
	155.0(7)	170.5(8)	163.1(5)		

(M-I) transition at $T_{MI}=360$ K (Refs. 14 and 25) and, presumably, with a structural transition.[18] It is worth recalling that this transition is not present for oxygen contents $\delta \geqslant 0.6$.[14] Below T_{MI}, a magnetic transition takes place at 275 K in which a net ferromagnetic component appears in the Co sublattice. This ferromagnetic component suddenly drops at $T_N=255$ K, coinciding with a small bump in the resistivity curve (*vide ultra*). For this FM-AFM transition, measurements following warming and cooling processes evidence hysteretic phenomena characteristic of a first-order transition. These $M(T)$ features are in agreement with previous results reported for $GdBaCo_2O_{5.5}$.[14,19] Ordering of Gd moments was not detected down to 2 K. Assuming that the low-temperature enhancement of $M(T)$ is exclusively due to the Gd atoms, it is possible to estimate the magnetic contribution of this specie [$M_{\text{Gd}}(T)\simeq 17.3\mu_B \text{K}/T$] in order to extract the contribution coming from Co ions: $M_{\text{Co}}(T) \equiv \frac{1}{2}[M(T)-M_{\text{Gd}}(T)]$. Figure 2 shows the inverse of the obtained results, in which the aforementioned singularity of $M(T)$ is now more pronounced. Between T_{MI} and T_C, the $M_{\text{Co}}(T)$ curve can then be analyzed using a simple Curie-Weiss law. The Curie temperature is estimated to be $\theta_C = 275\pm 3$ K$\cong T_C$ and the effective magnetic moment $\mu_{\text{eff(Co)}}=(1.9\pm 0.1)\mu_B$ per Co atom. Above T_{MI}, $\mu_{\text{eff(Co)}}$ increases considerably [$(4.3\pm 0.2)\mu_B$] and θ_C becomes negative ($\theta_C\cong -600$ K). Therefore, a magnetic transition, involving a drastic change in the sign of the exchange interactions between Co ions and in the amplitude of the paramagnetic moment, takes place associated to the electronic localization. Figure 3 displays the temperature dependence of the magnetization below RT for $\mu_0 H=0.5$, 1, 5, 8, and 10.5 T. The onset of long-range ferromagnetism (antiferromagnetism) shifts to higher (lower) temperatures under field. At the same time the stability range for the FM phase spreads out and the two sharp magnetic transitions in ZF become very rounded under increasing fields.

We will focus next on the high-field results. Figure 4 shows the isothermal magnetization measurements [$M(H)$] at $T=4.2$ and 100 K. Each isothermal curve was recorded after a zero-field-cooling process from RT down to the temperature of measurement. At low temperature, a two-step process of the magnetization is observed in connection to the two different magnetic ions (Gd and Co). At "low" fields, between 0 and 6–10 T, the moments of the paramagnetic Gd sublattice become fully polarized by the external field, with a magnetization $\Delta M_1=(7.8\pm 0.1)\mu_B$ per f.u. (or, equivalently, per Gd ion), which corresponds to the expected moment for Gd^{3+} ions. In addition to that, there is an hysteretic field-induced transition, which involves the Co sublattice, starting at a field of $\mu_0 H_C\sim 16.5$ T for $T=4.2$ K. The curvature of the magnetization indicates that the FM contribution of Co is practically saturated at the maximum field $\mu_0 H_C\sim 35$ T. On increasing temperature, the same magnetization process is

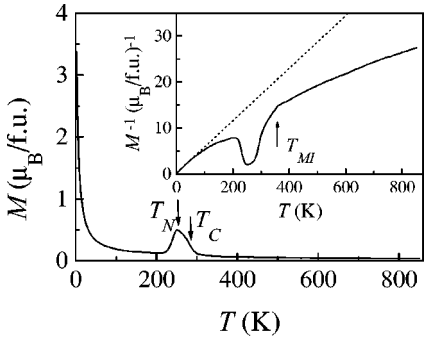

FIG. 1. Magnetization curve $M(T)$ of $GdBaCo_2O_{5.5}$ obtained under an applied field of 1 T. The inset presents the inverse of $M(T)$ (solid line) and the inverse of the contribution coming from Gd sublattice $M_{\text{Gd}}^{-1}(T)$ (dotted line).

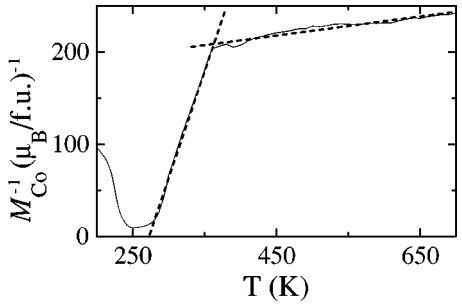

FIG. 2. Temperature evolution of the inverse magnetization coming from Co ions, $M_{Co}(T)$. Data correspond to that of Fig. 1 after subtracting the paramagnetic contribution of Gd ions. The dashed straight lines show the best fit of a Curie law in the intervals $T_c<T<T_{MI}$ and $T>T_{MI}$.

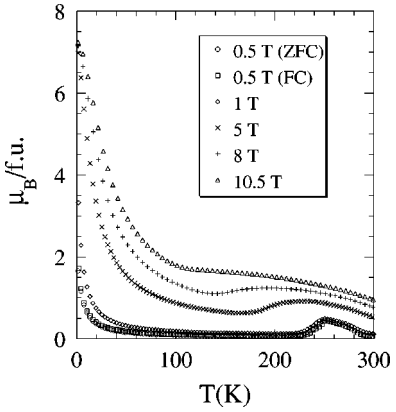

FIG. 3. Temperature dependence of the magnetization with applied field ranging from $\mu_0 H = 0.5$ T to 10.5 T.

observed with lower critical fields. H_C decreases down to $\mu_0 H_C \approx 11$ T at $T = 100$ K and the field transition disappears above $T_N = 255$ K. The hysteresis loops in this figure confirm a notable activation barrier between the AFM and FM phases of the Co sublattice. The average contribution of each Co ion, in the field-induced FM state, is around $\mu_{\mathrm{Co}} = (0.45 \pm 0.1)\mu_B$ and, within our resolution, remains constant, at least in the range of temperature 4.2 K$\leqslant T \leqslant$200 K $[\mu_{\mathrm{Co}} = (0.37 \pm 0.1)\mu_B$/Co ion at $T = 200$ K]. Above T_N and below T_C (not shown) the low-field magnetization curve, $M(H)$ are composed of a FM component due to the Co and a paramagnetic contribution arising from Gd and the fluctuating component of Co moment.

With the objective of investigating the correlation between the charge dynamics and the magnetic ordering, the resistivity as well as the optical transmission were measured as a function of magnetic field at several temperatures below RT. The magnetic-field dependence of the resistivity $\rho(H)$, measured in the longitudinal configuration, is illustrated in Fig. 5(a). The $\rho(H)$ measurements were performed after zero-field cooling following the same procedure as for the magnetization. The $\rho(H)$ curves reveal that, coinciding with the transition from the AFM to the FM state under field (Fig. 4), the resistivity shows a steep decrease. At $T = 4.2$ K, the resistivity displays an almost flat behavior up to $\mu_0 H \approx 15$ T, and then suddenly shows a steep decrease (about two orders of magnitude) which coincides with the FM arrangement of the Co ions. A similar behavior is observed at

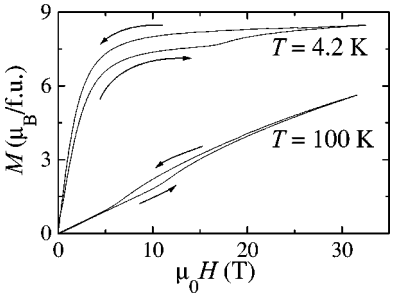

FIG. 4. Isothermal magnetization vs applied field curves evidencing the field-induced transition of the Co magnetic moment. This transition is not present for $T > T_N$.

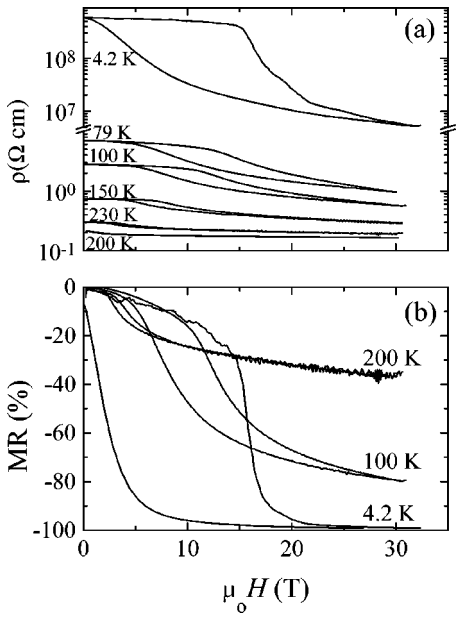

FIG. 5. (a) Isothermal resistivity vs applied field curves at temperatures (from top to bottom) 4.2, 79, 100, 150, 200, and 230 K. (b) Magnetoresistance vs applied field at 4.2, 100, and 200 K. This magnetoresistance disappears at T_N.

higher temperatures, with critical fields identical to those deduced from magnetization data. The field-induced transition vanishes at T_N. In the FM phase ($T_N < T < T_C$), a nonhysteretic linear magnetoresistance has been evidenced (not shown). The field-induced transition is of first order, accompanied by a wide hysteresis that increases at low temperatures due to suppression of the thermal fluctuations. A colossal magnetoresistance (CMR) effect takes place associated to the field-induced transition. The magnetoresistance as a function of magnetic field is shown in Fig. 5(b) at 4.2, 100, and 200 K. Data according to the definition MR(%) $= 100 \times [\rho(T, \mu_0 H = 32\ \mathrm{T}) - \rho(T, \mu_0 H = 0)]/\rho(T, \mu_0 H = 0)$ have been deduced from Fig. 5(a). Pronounced and sudden field-induced changes were also evidenced by optical transmission measurements versus the magnetic field up to 30 T. They are shown in Fig. 6, where each curve corresponds to the sample transmission measured during the pulsed field $[\tilde{T}(H)]$ at a frequency $f = 344$ GHz. The monotonous variation of the transmission present the same features as the resistivity ones. It suddenly decreases at the field-induced transition and

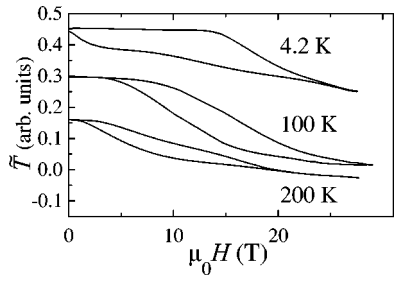

FIG. 6. Isothermal optical transmission vs applied field measured with $f = 344$ GHz.

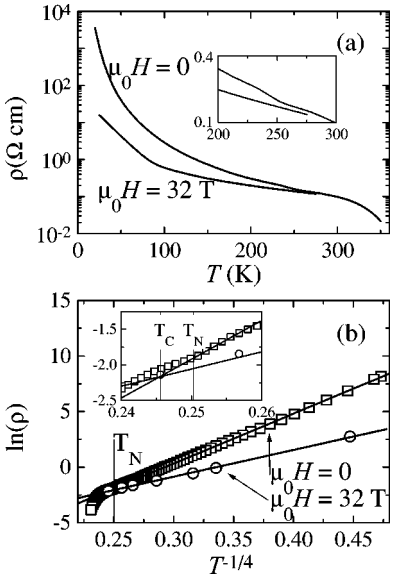

FIG. 7. (a) Temperature dependence of the resistivity without applied field and under $\mu_0 H = 32$ T. (b) Plot of $\ln \rho(T, \mu_0 H = 0$ T) (circles) and $\ln \rho(T, \mu_0 H = 0$ T) (squares) (ρ in Ω cm) vs $T^{-1/4}$ (T in K); the straight lines are the best fit of Eq. (1). Both insets show in detail the temperature range around T_N and T_C.

shows the same critical fields as those observed for the magnetization and the resistivity.

Figure 7(a) displays the resistivity measured in ZF and under 32 T. It should be emphasized that lower resistivity values are obtained under field below $T_N = 255$ K. At this temperature, the applied magnetic field makes the small bump exhibited by $\rho(T, \mu_0 H = 0)$ to disappear. It is apparent that the MR in $GdBaCo_2O_{5.5}$ is associated to the disruption of the Néel phase by the field and vanishes at T_N.

IV. DISCUSSION

The functional dependence of both $\rho(T, \mu_0 H = 0)$ and $\rho(T, \mu_0 H = 32$ T) is well described for $T < T_N$ by Mott's variable-range hopping (VRH) model, according to the law

$$\rho = \rho_0 \exp\left(\frac{T_0}{T}\right)^{1/4}. \tag{1}$$

The corresponding resistivity fits for $\mu_0 H = 0$ and $\mu_0 H = 32$ T are shown in Fig. 7(b). Other exponents different to 1/4 were tested as well without satisfactory results. Above T_N, the limited temperature range investigated does not permit unambiguous determination of the carrier transport mechanism. A significant feature of $\rho(T, \mu_0 H = 0)$ is a sudden small bump coinciding with T_N. It is apparent from Figs. 7(a) and 7(b) that the scattering mechanism suppressed by the application of a high magnetic field is the same producing the reduced carrier mobility in the system when enters the AFM phase. From the fitted values of T_0 in Eq. (1), the hopping range of the carriers in the FM state is about 12 times larger than in the AFM state. This confirms the interplay between carrier hopping and the localized Co moments.

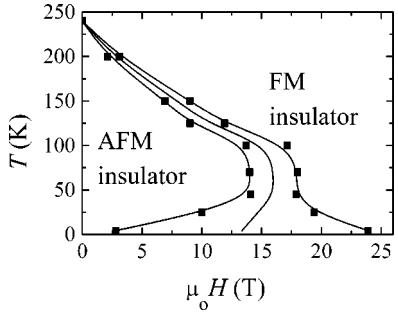

FIG. 8. $\mu_0 H$-T phase diagram obtained from magnetization measurements. The solid lines are guides to the eyes.

The sudden changes of the isothermal $M(H)$, $\rho(H)$, and $\tilde{T}(H)$ curves at a certain applied field evidence that, below T_N, $GdBaCo_2O_{5.5}$ presents a first-order field-induced transition. The hysteretic behavior allows us to define the transition field H_C^+ (H_C^-) which corresponds to the field at which the derivative of the magnetization dM/dH reaches its maximum value in the sweep-up (-down) process. Figure 8 shows the $\mu_0 H$-T phase diagram obtained from this definition. The thermodynamic field defined as $H_C \equiv (H_C^+ + H_C^-)/2$ displays a maximum value of 16 T at $T \approx 75$ K.

At 4.2 K the first stage of the magnetization upturn is completely finished at ≈ 16.5 T and the value of the magnetization just below this field corresponds to the magnetic moment expected for a fully polarized array of Gd^{3+} ions. This evidences that the ''second jump'' in the $M(H)$ curve exclusively comes from the Co sublattice. In the magnetization curve at 4.2 K the disruption of the AFM ordering renders a phase with a FM component. The saturation of the magnetization shown in Fig. 4 is compatible with a magnetic moment of $(0.45 \pm 0.1)\mu_B$ per Co ion. We have not detected appreciable changes in this value in the interval 4.2–200 K (above the last temperature our lack of accuracy precludes any conclusion). It is of interest to recall here that Moritomo *et al.*[18] refined the magnetic intensity diffracted by $TbBaCo_2O_{5.5}$ at 50 K in zero field. Assuming a layered AFM spin structure, they estimated the Co moment to be $\sim 0.4(2)\mu_B/Co$. Although this value agrees with the FM component observed in our Gd sample after the field transition, the rough estimation by Moritomo *et al.*[18] was based on a single weak magnetic Bragg peak $(0\ 0\ \frac{1}{2})$. From the structural point of view, $GdBaCo_2O_{5.5}$ crystallizes in the $P\,mmm$ space group, with two distinguishable Co positions (pyramids and octahedra). Numerically, $(0.45 \pm 0.1)\mu_B/Co$ does not correspond to a 50%-50% mixture of LS and HS ($2\mu_B/Co$, in the hypothesis of a null orbital moment) or to a 50%-50% mixture of LS and IS ($1\mu_B/Co$, in the same hypothesis). In this context, there are two possible scenarios in which the magnetic moment of Co ions at low temperature would be larger than $(0.45 \pm 0.1\mu_B)$. The first one is that the state at high field corresponds to a weak FM phase. The second one is that this state corresponds to a ferrimagnetic phase. The curvature of $M(H)$ line at $\mu_0 H = 32$ T is against the weak FM hypothesis, but present data do not permit us to rule out the second scenario. Nevertheless, as discussed be-

low, the effective paramagnetic moment of Co ions in the region $T_C < T < T_{MI}$ ensures that a significant fraction of Co^{3+} ions are in LS state at low temperature.

On the contrary, two extra contributions to the magnetic moment have to be considered: first (already mentioned), a possible orbital contribution to the observed ferromagnetic moment and second, the possibility of having a certain contribution from Co^{4+} moments due to an oxygen concentration slightly above 5.5 (permitted by our error bars). The first possibility requires more specific investigations as an orbital moment $m_L = 1.04\mu_B$ has been predicted for Co^{3+} ions in $YBaCo_2O_5$.[21] On the other hand, the AFM phase cannot be based on the presence of Co^{4+} moments due to an oxygen concentration slightly above 5.5 (in our case the Co^{4+}:Co^{3+} ratio is smaller than 7%:93%). In such a scenario (all Co^{3+} in the LS state, $m=0$, and Co^{4+} in the HS state, $m=5\mu_B$) one should expect absence of long-range ordering, specially at temperatures as high as $T_N = 240$ K.

The sharp change in the slope of the $M_{Co}^{-1}(T)$ curve at $T_{MI} \approx 360$ K, which can be clearly appreciated in Fig. 2, has also been observed in other samples with $\delta \approx 0.5$.[14,18] Moritomo *et al.*[18] have interpreted it as an evidence of a change in the spin state of the Co^{3+} ions from IS ($T < T_{MI}$) to HS ($T > T_{MI}$). Besides, Maignan *et al.*[14] have proposed a spin-state-ordered scheme below T_{MI}, LS in octahedral CoO_6 sites and IS in pyramidal CoO_5 sites, and an evolution towards the full HS state above T_{MI}. Between T_C and T_{MI}, in our sample we have obtained $\mu_{\mathrm{eff(Co)}} = 1.9(1)\mu_B$, which agrees with the IS-LS scheme (predicted as $2\mu_B$).[26]

An estimation of the effective magnetic moment in the metallic ($T > T_{MI}$) regime renders $\mu_{\mathrm{eff}}(\mathrm{Co}) = 4.3(1)\mu_B$ (Fig. 2), consistent with the 50% of Co in IS and the other 50% in the HS spin states. This is the expected spin-state scheme at high temperatures (from entropic considerations),[27] as reported to happen in $LaCoO_3$.[3,9] However, at variance with $LaCoO_3$, the presence of two Co sites perfectly ordered in the present case makes the ordered IS-HS scheme in the metallic phase very plausible.

The insulating character of the FM state induced by the magnetic field (Fig. 7) is consistent with the existence of a FM insulating state in zero field between T_N and T_C. However, discerning whether they correspond or not to the same electronic configuration is not possible from present data. Both exhibit a weak FM component but the VRH law describing the temperature dependence of $\rho(T, \mu_0 H = 32$ T) fails to describe the resistivity in the zero-field FM region [see inset of Fig. 7(b)].

V. CONCLUSIONS

We have investigated the relationship between magnetic ordering and conductivity in the Co^{3+} compound $GdBaCo_2O_{5.5}$. Synchrotron x-ray powder diffraction data confirmed the high quality of the sample investigated and have provided a description of the ordered arrangement of CoO_6 octahedra and CoO_5 pyramids in a cell with $P\,mmm$ structural symmetry.

The resistivity and optical transmission of this oxide were measured as a function of temperature below RT and as a function of pulsed magnetic fields of up to 35 T. M, ρ, and $\tilde{T}$ data collected under high fields have permitted us to establish the $\mu_0 H$-T phase diagram for $GdBaCo_2O_{5.5}$. A first-order field-induced transition has been observed below T_N. The thermodynamic critical field is $\mu_0 H \approx 16$ T at low temperature. Our measurements evidence that the contribution of Co ions to the FM moment in the high-field state corresponds to $(0.45 \pm 0.1)\mu_B$/Co ion, without appreciable changes between 4.2 K and close below T_N. This value is smaller than the expected from a 50% mixture of LS and IS ($1\mu_B$/Co ion), though the paramagnetic Co moment between T_C and T_{MI} is consistent with such a mixture. Therefore, it cannot be discarded that high-field state correspond to a ferrimagnetic phase. Steep changes in the conductivity and the magnetoresistance are also observed during the first order field transition. The scattering mechanism inhibited by the application of field ($H > H_c$) seems to be the same mechanism responsible for the reduction of the carrier mobility across the FM to AFM transition on cooling the sample in zero field. Consequently, the high-field phase is probably very similar in nature to the zero-field FM phase.

ACKNOWLEDGMENTS

The authors thank Dr. J. Fontcuberta for fruitful discussions. Financial support by the CICyT (Spanish Government, MAT97-0699 and MAT1999-0984-C03-01), MEC (Spanish Government, PB97-1175), CIRIT (Generalitat de Catalunya, GRQ95-8029), and the EC through the ''Oxide Spin Electronics (OXSEN)'' network (TMR) is acknowledged. The provision of beam time at ESRF is acknowledged.

[1] W.C. Koehler and E.O. Wollan, J. Phys. Chem. Solids **2**, 100 (1957).
[2] J.B. Goodenough, J. Phys. Chem. Solids **6**, 287 (1958).
[3] M.A. Señaris-Rodríguez and J.B. Goodenough, J. Solid State Chem. **116**, 224 (1995).
[4] G. Thornton, B.C. Tofield, and A.W. Hewat, J. Solid State Chem. **61**, 301 (1986).
[5] M. Zhuang, W. Zhang, and N. Ming, Phys. Rev. B **57**, 10 705 (1998).
[6] M.A. Korotin, S.Yu. Ezhov, I.V. Solovyev, V.I. Anisimov, D.I. Khomskii, and G.A. Sawatzky, Phys. Rev. B **54**, 5309 (1996).
[7] T. Saitoh, T. Mizokawa, A. Fujimori, M. Abbate, Y. Takeda, and M. Takano, Phys. Rev. B **55**, 4257 (1997).
[8] S. Yamaguchi, Y. Okimoto, and Y. Tokura, Phys. Rev. B **55**, R8666 (1997).
[9] K. Asai, A. Yoneda, O. Yokokura, J.M. Tranquada, G. Shirane, and K. Kohn, J. Phys. Soc. Jpn. **67**, 290 (1998).
[10] C. Martin, A. Maignan, D. Pelloquin, N. Nguyen, B. Raveau, Appl. Phys. Lett. **71**, 1421 (1997).
[11] I.O. Troyanchuk, N.V. Kasper, D.D. Khalyavin, H. Szymczak, R. Szymczak, and M. Baran, Phys. Rev. Lett. **80**, 3380 (1998).
[12] I.O. Troyanchuk, N.V. Kasper, D.D. Khalyavin, H. Szymczak, R.

Szymczak, and M. Baran, Phys. Rev. B **58**, 2418 (1998).
[13] Y. Moritomo, M. Takeo, X.J. Liu, T. Akimoto, and A. Nakamura, Phys. Rev. B **58**, R13 334 (1998).
[14] A. Maignan, C. Martin, D. Pelloquin, N. Nguyen, B. Raveau, J. Solid State Chem. **142**, 247 (1999).
[15] E. Suard, F. Fauth, and V. Caignaert, Physica B **276-278**, 254 (2000).
[16] T. Vogt, P.M. Woodward, P. Karen, B.A. Hunter, P. Henning, and A.R. Moodenbaugh, Phys. Rev. Lett. **84**, 2969 (2000).
[17] E. Suard, F. Fauth, V. Caignaert, I. Mirebeau, and G. Baldinozzi, Phys. Rev. B **61**, R11 871 (2000).
[18] Y. Moritomo, T. Akimoto, M. Takeo, A. Machida, E. Nishibori, M. Takata, M. Sakata, K. Ohoyama, A. Nakamura, Phys. Rev. B **61**, R13 325 (2000).
[19] W.S. Kim, E.O. Chi, H.S. Choi, N.H. Hur, S.-J. Oh, and H.-C. Ri, Solid State Commun. **116**, 609 (2000).
[20] H. Wu, Phys. Rev. B **62**, R11 953 (2000).
[21] S.K. Kwon and B.I. Min, Phys. Rev. B **62**, R14 637 (2000).
[22] H. Kuwahara, Y. Tomioka, A. Asamitsu, Y. Moritomo, and Y. Tokura, Science **270**, 961 (1995).
[23] M. Tokunaga, N. Miura, Y. Tomioka, and Y. Tokura, Phys. Rev. B **57**, 5259 (1998).
[24] M. Respaud, A. Llobet, C. Frontera, C. Ritter, J.M. Broto, H. Rakoto, M. Goiran, and J.L. García-Muñoz, Phys. Rev. B **61**, 9014 (2000).
[25] In Ref. 11 the air-synthesized sample of $GdBaCo_2O_{5+\delta}$ studied, which the authors assumed (without an oxygen content analysis) to have $\delta=1$, can be assumed, from results of Ref. 14, to have $\delta\approx 0.5$.
[26] Considering spin-only contributions to the effective paramagnetic moment.
[27] At high enough temperature, the population of each spin state can be expected to be proportional to its degeneracy. The degeneracies are 1, 18, and 15 for LS, IS, and HS states, respectively.